The age, petrography, geochemistry and tectonic setting of the late Caledonian Gåsøy Intrusion, west Norway

H. FURNES, R. B. PEDERSEN, B. SUNDVOLL, M. TYSSELAND & O. TYMYR

Furnes, H., Pedersen, R. B., Sundvoll, B., Tysseland, M. & Tymyr, O.: The age, petrography, geochemistry and tectonic setting of the late Caledonian Gåsøy Intrusion, west Norway. *Norsk Geologisk Tidsskrift*, Vol. 69, pp. 273–289. Oslo 1989. ISSN 0029–196X.

The Gåsøy Intrusion of gabbronorite and diorite is situated in the westernmost Norwegian Caledonides. A Sm–Nd mineral isochron on a diorite has given an age of 380 ± 26 Ma. In the easternmost part of the pluton a gradual change can be demonstrated in the mineral and whole-rock geochemistry from a massive and layered gabbronorite to a highly-differentiated diorite as well as granitic rocks at its margin. Geochemically the intrusion is subalkaline and its trace-element pattern is typical of a subduction-related environment. Mass-balance calculations based on observed mineral data suggest that the diorites were derived by fractional crystallization from a basaltic parent. Initially, plagioclase and orthopyroxene with lesser amounts of olivine and clinopyroxene were fractionated. In the production of the quartz-bearing diorites, fractionation of plagioclase and clinopyroxene with less olivine and minor ilmenite was operative. Evidence of crustal contamination and magma mixing is given by Sr-isotopes and zoned plagioclase.

H. Furnes, R. B. Pedersen, M. Tysseland & O. Tymyr, Geologisk Institutt, Avd. A, Allégt. 41, N–5007 Bergen, Norway; B. Sundvoll, Mineralogisk-Geologisk Museum, Sarsgt. 1, Oslo 5, Norway.

The southern end of Frøya and adjacent islands and skerries to the west and southwest comprise an intrusive body, the Gåsøy Intrusion (GI) (Fig. 1). The exposed part of the intrusion is composed of unaltered gabbronorites and subordinate ultramafic and felsic rocks. A brief petrographic description of the gabbronorite was given by Kolderup (1928). To the north and northeast diorites grade into quartz-bearing diorites (Fig. 1). On the southern end of Frøya, quartz-diorites and granites of the GI are in intrusive contact with a sedimentary melange, the Kalvåg Melange, in which metapelites have been metamorphosed to biotite-quartz hornfels with porphyroblasts of altered andalusite, staurolite and cordierite (Bryhni & Lyse 1985). The Kalvåg Melange is unconformably overlain by Devonian sediments, but its lower age limit is so far unknown. Reusch (1903) and Kolderup (1928) reported fossils of probable Ordovician–Silurian age, but this has not been confirmed. A tenuous line of evidence suggests, however, an age younger than that of the Solund–Stavfjord Ophiolite Complex, dated by U/Pb on zircons to 443 ± 3 Ma (Dunning & Pedersen 1988).

In this study we present Sm–Nd and Rb–Sr ages as well as whole-rock and mineral geochemistry of the Gåsøy Intrusion. Finally, we discuss the petrogenesis of the gabbronorite and diorites and how they may be related to each other by fractional crystallization.

The Gåsøy Intrusion

General description

The gabbronorite exposed on the southern half of the archipelago (Fig. 1) is generally massive, medium to coarse grained, with minor occurrences of pegmatite and thin felsic veins and pods. Basic xenoliths occur within the massive part. On some of the islands, e.g. Gåsøy and Torbjørnholmen (Fig. 1), the gabbronorite shows a faint, steeply-dipping modal lamination (Fig. 2A). Well-developed modal layering is rare but has been observed on one of the small islands south of Værøy (Fig. 2B). On the island of Gåsøy wehrlite occurs interlayered with gabbronorite and diorite. The diorite is in general massive and coarse grained. Because of limited exposure it is impossible to provide a three-dimensional structure of the GI. However, the distribution of rock types (Fig. 1) suggests that the partly layered gab-

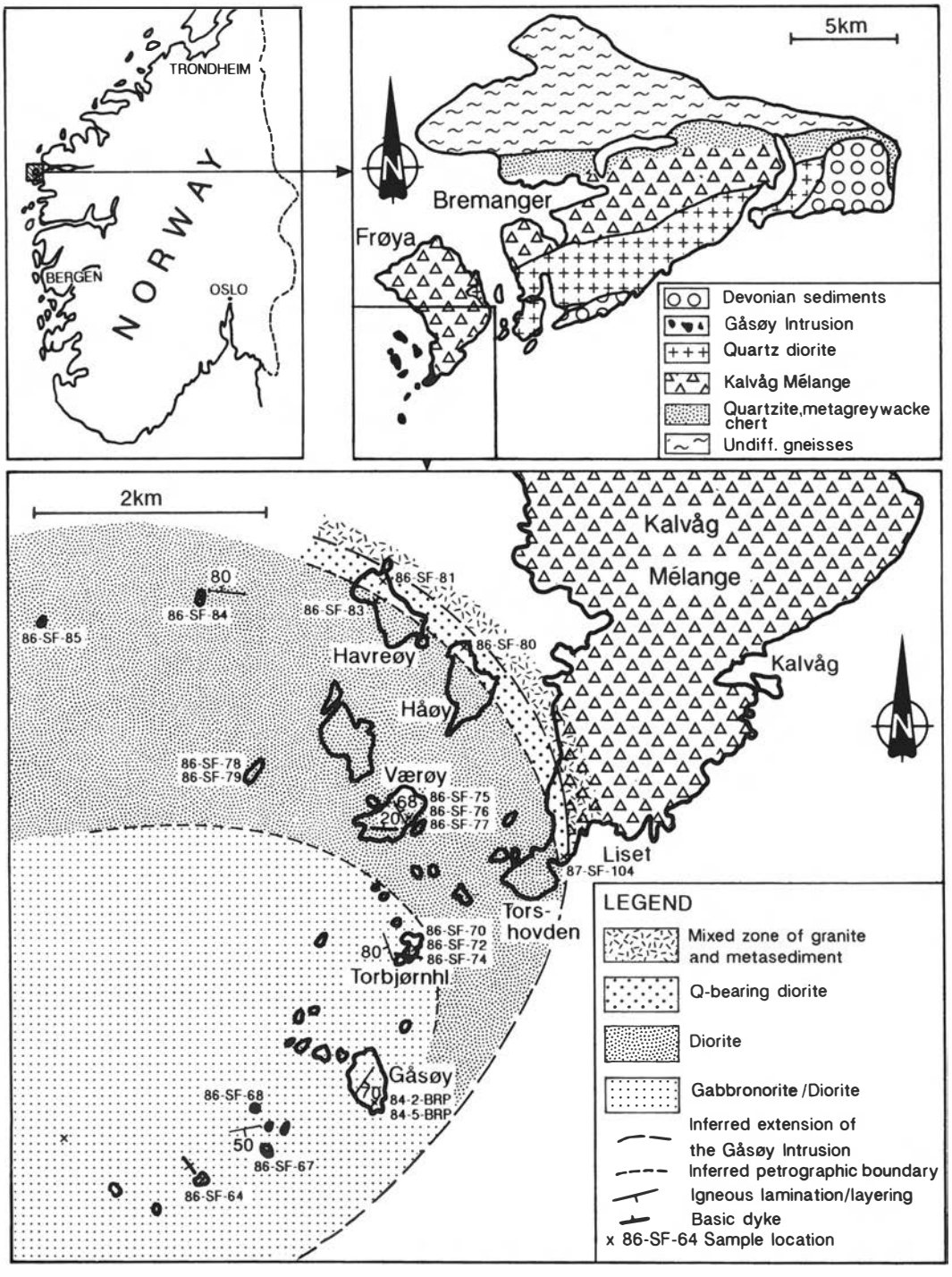

Fig. 1. Geological map of the Gåsøy Intrusion and its host.

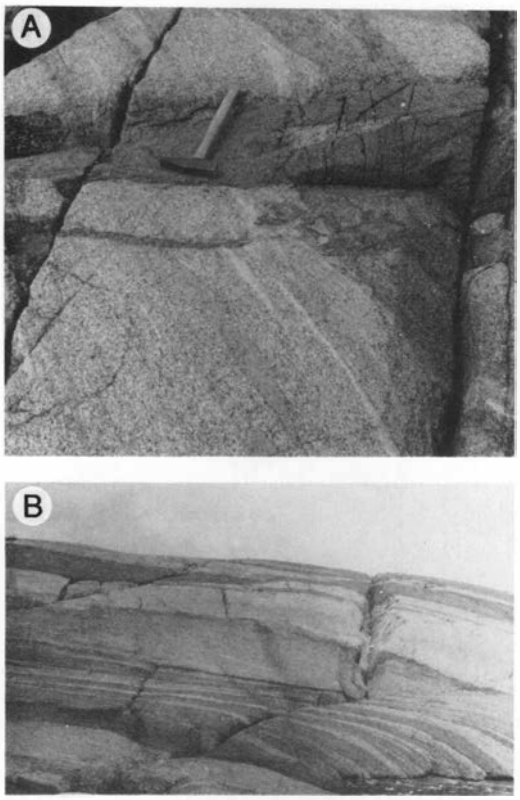

Fig. 2. A. Laminated gabbronorite cut by basic dyke. Location: Torbjørnhl. B. Layered gabbronorite/diorite. Location: Small island about 500 m south of Værøy.

bronorites in the southern part (Fig. 1) represent the lowermost exposed part of the intrusion. The rocks of the GI do not show any foliation, and appear to be undeformed. The GI is cut by basic dykes. The few examples that have been found cut the banding/layering at a high angle (Figs. 1, 2A). The dykes do not have chilled margins, but 1–2 cm thick reaction zones in which pyroxene is converted to brown amphibole are common between the dyke walls and the host.

Contact relations with the host

The contact between the GI and the Kalvåg Melange can be studied on the southwestern part of Frøya and on the northern tip of Havreøy (Fig. 1). At a distance of about 150 m from the quartz-bearing diorites (Fig. 1), thin (a few mm thick) acid rootless veins make their first appearance in the metapelitic rocks of the melange. Nearer the intrusion the numbers of acid veins and lenses increase, and they most probably represent partial melts of the metasediments. Some of the veins are foliated and folded together with the metasediments (Fig. 3A), whereas in other cases they disrupt earlier veined and deformed metapelites (Fig. 3B). In the case of more extensive collection of acid melts into cm-thick irregular bodies and sheets, they appear undeformed. These apparently undeformed acid bodies, in some cases containing remnants of paleosome, may, however, grade into, or cut sharply across, veined and strongly deformed metasediments (Fig. 3C). Granitic pods and veins are also found in the quartz-bearing diorites (Fig. 3D). These relations show that the emplacement of the GI took place contemporaneously with, or subsequent to the deformation of the Kalvåg Melange.

Age determinations

Rb–Sr and Sm–Nd age determinations of the GI have been carried out in the isotope laboratory at the Mineralogical–Geological Museum, University of Oslo. The analytical procedures and instrumental performances are similar to those described by Mearns (1986). The analytical data are presented in Table 1 and the resulting isochron fits in Fig. 4. The most reliable results are represented by a Sm–Nd isochron based on mineral separates (clinopyroxene, plagioclase, plagioclase + apatite) from diorite 86–SF–83 (Fig. 1). The isochron fit of these data (Fig. 4a) yielded an age of 380 ± 26 Ma (MSWD = 1.98). An identical result is obtained by a Rb–Sr isochron based on plagioclase, apatite and clinopyroxene mineral separates of sample 86–SF–83, combined with whole-rock samples of 86–SF–76 and 86–SF–83, which yields an age of 390 ± 29 Ma (MSWD = 1.8) (Fig. 4b). These ages indicate crystallization in the late Silurian or Devonian. Sample 86–SF–83 has yielded the highest εNd (2.5) and lowest εSr (−4.5), indicating that it represents the most primitive or least contaminated material of the intrusion, and hence has been chosen as the most reliable for age determination. Acid veins (86–SF–74, 86–SF–77 and 86–SF–79), together with one of the quartz-bearing diorites (86–SF–81), define a poor isochron of 411 ± 30 Ma (MSWD = 3.9) and with an εSr of ca. 18 and an εNd of ca. −1. If comagmatic with the basaltic magma, the felsic dykes and veins and the marginal quartz-bearing diorites have been contaminated with a

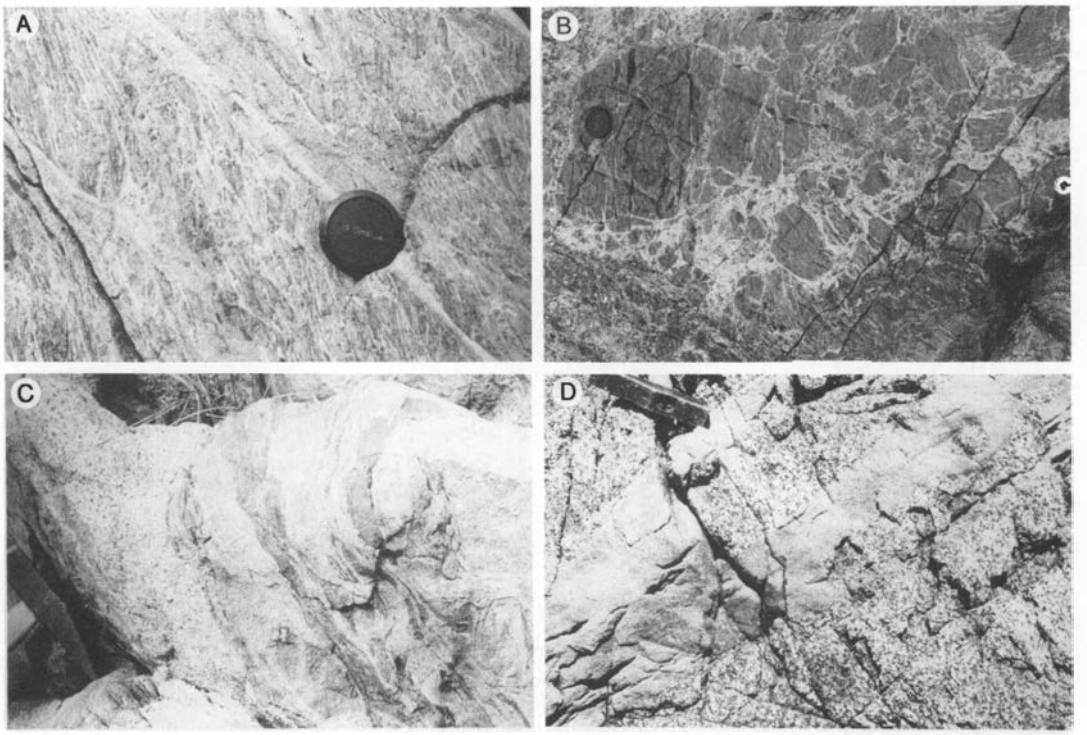

Fig. 3. Contact relations between the Gåsøy Intrusion and its host (the Kalvåg Melange). A. Network of thin acid veins, presumably generated by partial melting of the metapelite host. Note that the veins are strongly deformed. Ca. 100 m from the contact with the diorites of the GI. B. Network of acid veins cutting disrupted metapelite. C. Granite veins with slivers of metapelite. D. Granite vein cutting quartz-bearing diorite. Locations: Photos A, C and D: Contact area between Torshovden and Liset. Photo B: Little peninsula on the northernmost tip of Havreøy (see Fig. 1).

crustal component. The other samples analysed have yielded εNd and εSr values approximately between the limits indicated (Table 1).

Petrography

The gabbronorites and diorites are medium to coarse-grained, occasionally pegmatititc rocks, with crystal shapes ranging from subhedral to anhedral. The gabbronorites are distinguished from the diorites on the basis of basic plagioclase composition, i.e. An > 50 = gabbronorite, An < 50 = diorite. The plagioclase and olivine crystals are dominantly subhedral to anhedral, whereas pyroxene, Fe–Ti oxides, amphibole and biotite are usually anhedral, though orthopyroxene frequently occurs as euhedral to subhedral crystals. Igneous lamination is common, but subophitic textures are observed in many samples. Apart from plagioclase crystals of variable size, the rocks are dominantly equigranular. The minerals of the gabbronorite are fresh, whereas in the more differentiated diorites and quartz-bearing diorites the margin of the intrusion hydrothermal alteration may be quite pronounced. This is expressed in clouding of plagioclase, conversion of orthopyroxene into bastite, and amphibole growth on the margins of clinopyroxene. Biotite may occur as individual crystals, but are common around Fe–Ti oxides. From textural relationships the crystallization sequence appears to be: olivine – Fe–Ti–oxide – plagioclase – orthopyroxene – clinopyroxene – amphibole – biotite – quartz. Apatite, zircon and sphene appear in the diorites and quartz-bearing diorites as minor constituents.

Mineral chemistry

Electron-microprobe analyses were carried out using an ARL SEMQ in the Geological Institute, University of Bergen, employing standard wave-

Table 1. Analytical data of mineral separates and bulk rock.

	Sm (ppm)	Nd (ppm)	147Sm/144Nd	143Nd/144Nd	εNd (T = 380)
86SF83					
Clinopyroxene	10.14	31.01	0.199141	0.512796 ± 4	2.79
Plagioclase	1.45	8.44	0.104519	0.512559 ± 4	2.76
Plag. + apatite	29.90	131.75	0.136793	0.512647 ± 4	2.91
86SF81 (bulk)	10.25	43.56	0.14333	0.512465 ± 5	−0.96
86SF85 (bulk)	3.18	12.84	0.15074	0.512591 ± 5	1.14
	Rb (ppm)	**Sr (ppm)**	**87Rb/86Sr**	**87Sr/86Sr**	**εSr (T = 380)**
86SF83					
Clinopyroxene	7.69	91.95	0.24204	0.705070 ± 30	−4.23
Plagioclase	24.84	503.34	0.14271	0.704500 ± 30	−4.70
Plag. + apatite	18.29	487.55	0.10851	0.704370 ± 30	−3.91
86SF85 (bulk)	13	439	0.08566	0.705290 ± 30	10.91
86SF68 (bulk)	2	310	0.01866	0.704250 ± 30	1.29
86SF84 (bulk)	20	427	0.13547	0.704810 ± 30	0.26
86SF83 (bulk)	20	340	0.17014	0.704700 ± 30	−3.96
78SF78 (bulk)	15	373	0.11631	0.704310 ± 30	−5.37
86SF76 (bulk)	6	449	0.03865	0.703950 ± 30	−4.51
86SF81 (bulk)	83	271	0.88634	0.710390 ± 30	21.81
86SF74 (bulk)	56	584	0.27741	0.706890 ± 30	18.90
86SF77 (bulk)	60	446	0.38921	0.707540 ± 30	19.54
86SF79 (bulk)	54	546	0.28612	0.706820 ± 30	17.23

length dispersive techniques (Reed 1975), an accelerating voltage of 15 KV, and a beam current of 10 nA. Well-characterized minerals, synthetic oxides and pure metals were employed as standards. Net peak intensities, corrected for dead-time effects and beam-current drift as monitored from the objective aperture, were reduced by MAGIC IV (Colby 1968).

A large number of electron microprobe analyses of olivine (2), plagioclase (222), orthopyroxene (84), clinopyroxene (81), Fe–Ti oxide (32), amphibole (25) and biotite (40) have been carried out, and representative analyses of each mineral are shown in Table 2. A more comprehensive list of analyses is available on request from the senior author.

Olivine as a fresh mineral is only present in gabbronorite. A representative analysis of olivine in sample 86–SF–67 gives a Fo-content of around 69 (Table 2).

Pyroxene. Both clinopyroxene and orthopyroxene are present throughout the intrusion. A significant compositional variation from Fe-poor to Fe-rich pyroxenes can be demonstrated (Fig. 5, Table 2). Pyroxene compositions are also shown on the map of Fig. 8.

Plagioclase. The plagioclase compositions show marked differences from An 69.5 in the most-primitive gabbronorite to An 22.5 in the most-differentiated quartz-bearing diorite (Fig. 6, Table 2). Within each sample there is a marked variation in the An content, ranging from 4.6 to 20.9 mol% An in samples 86–SF–67 and 86–SF–85, respectively (Fig. 6). Normal as well as oscillatory and reverse zoning is common in the plagioclase (Fig. 7). In some of the quartz-bearing diorite samples (86–SF–81) as well as in the granites, mantled feldspars, showing a core of strongly sericitized K-feldspar overgrown by plagioclase, are common.

Biotite. The composition of biotite changes progressively from a Mg-rich/Fe-poor type in the gabbronorite to a Mg-poor/Fe-rich type in the quartz-bearing diorite (Fig. 8, Table 2).

Amphibole. According to the classification to Leake (1978), the amphibole can be classified as ferroan paragasite, magnesio-hornblende, edenite, ferroedenitic hornblende and ferro-horn-

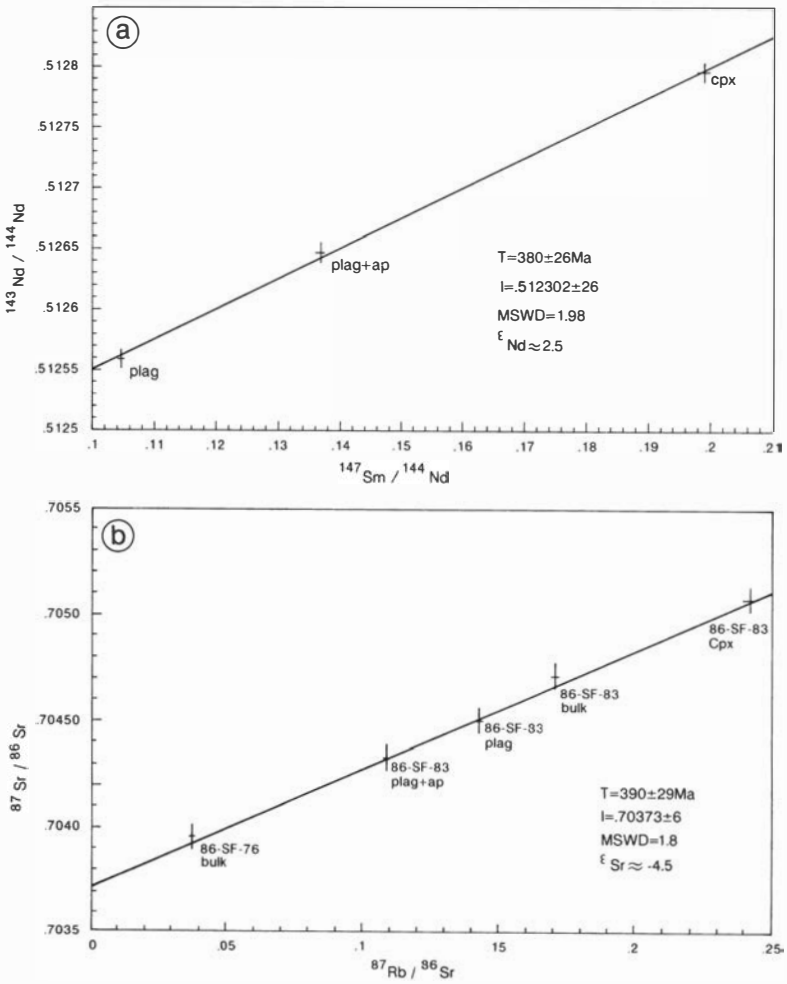

Fig. 4. Isochron fits of Sm–Nd and Rb–Sr isotope data from the Gåsøy Intrusion. Errorbars indicate 2σ errors. A. Sm–Nd isochron plot based on clinopyroxene (cpx), plagioclase (plag) and plagioclase + apatite (plag + ap) separates from diorite 86–SF–83. B. Rb–Sr isochron plot based on clinopyroxene (cpx), plagioclase (plag) separates of diorite 86–SF–83, bulk-rock samples of 86–SF–76 and 86–SF–83.

blende. There is, as demonstrated for the minerals described above, a systematic change in composition from gabbronorites to the quartz-bearing diorites. The gabbronorites and the least-differentiated diorites contain ferroan pargasite, magnesio-hornblende and edenite, whereas in quartz-bearing diorites ferroendenitic hornblende and ferro-hornblende occur (Table 2).

Fe–Ti oxide. All the analysed Fe–Ti oxide crystals are ilmenite (Table 2). In the least-fractionated diorites (sample 86–SF–84) and quartz-bearing diorites (samples 86–SF–80 and 86–SF–81), ilmenite shows little compositional variation.

Whole-rock geochemistry

The whole-rock geochemical analyses were carried out using a Philips PW 1450 automatic X-ray fluorescence spectrometer at the Geological Institute, University of Bergen. The glass-bead technique of Padfield & Gray (1971) was used for the major elements and pressed-powder pellets for the trace elements using international basalt standards for calibration and Flanagan's (1973) recommended values.

To present meaningful whole-rock analyses for petrogenetic consideration each sample should ideally represent a liquid composition. Such conditions are, in this case, not fully achieved, because of possible cumulative effects. The samples used (Table 3), however, have been carefully selected on the basis of their textures and major- and trace-element characteristics from a larger data base. Thus, samples which on this basis show clear evidence of representing cumulates have been excluded from the further discus-

Table 2. Mineral analyses of the Gåsøy Intrusion used in petrographic-mixing calculations.

	Ol	Opx	Cpx			
	86SF67	86SF67	86SF68	86SF78	86SF81	87SF104
SiO_2	37.70	54.79	52.98	51.32	50.68	50.47
TiO_2		0.07	0.95	0.50	0.29	0.06
Al_2O_3		1.18	2.80	2.01	0.98	0.70
Cr_2O_3		0.03	0.22	0.14	0.04	0.03
FeO*	28.26	16.73	6.93	10.62	15.74	16.76
MnO	0.50	0.42	0.12	0.28	0.40	0.38
MgO	35.52	27.28	17.01	13.54	10.18	8.97
CaO	0.04	1.44	21.17	20.84	19.81	20.60
Na_2O		0.08	0.27	0.37	0.27	0.34
Total	102.62	100.98	102.45	99.51	98.39	98.10
0 =	4	6		6		
Si	0.985	1.966	1.906	1.914	1.978	1.987
Ti		0.002	0.026	0.020	0.009	0.002
Al		0.050	0.119	0.107	0.045	0.033
Cr		0.001	0.006	0.004	0.001	0.003
Fe	0.631	0.502	0.208	0.336	0.514	0.552
Mn	0.011	0.013	0.004	0.009	0.013	0.013
Mg	1.383	1.443	0.912	0.763	0.592	0.526
Ca	0.001	0.027	0.816	0.844	0.828	0.869
Na		0.005	0.019	0.027	0.020	0.026
Mg/(Mg + Fe)	0.687					
X		2.00	2.00	2.00	2.00	2.00
WXY		2.01	2.02	2.02	2.00	2.01
En		73.2	47.1	39.3	30.6	27.0
Fe		25.4	10.8	17.3	26.6	28.3
Wo		1.4	42.1	43.3	42.8	44.7
	Plagioclase				Amphibole	
	86SF67	86SF75	87SF104	86SF81	86SF85	86SF81
SiO_2	53.04	58.72	62.05	61.35	45.75	42.52
TiO_2					1.34	1.37
Al_2O_3	29.40	26.31	24.99	24.44	8.52	9.48
Cr_2O_3					0.00	0.08
FeO*					16.16	23.04
MnO					0.37	0.30
MgO					13.24	8.70
CaO	12.08	8.28	6.47	5.44	10.63	9.80
Na_2O	4.46	6.74	7.78	8.31	1.49	0.93
K_2O	0.06	0.17	0.09	0.17	0.44	0.81
Total	99.04	100.22	101.38	99.71	97.95	97.03
0 =		32			23	
Si	9.679	10.470	10.861	10.912	6.777	6.592
Ti					0.149	0.160
Al	6.324	5.528	5.156	5.124	1.488	1.732
Cr					0.000	0.010
Fe					2.001	2.986
Mn					0.047	0.039
Mg					2.924	2.011
Ca	1.036	1.582	1.213	1.036	1.687	1.627

Table 2. (continued)

	Plagioclase				Amphibole	
	86SF67	86SF75	87SF104	86SF81	86SF85	86SF81
Na	1.576	2.331	2.642	2.865	0.429	0.280
K	0.013	0.038	0.020	0.040	0.084	0.160
Mg/(Mg + Fe)					0.59	0.40
Z	16.003	15.998	16.017	16.036		
X	3.951	3.951	3.875	3.941		
Ab	39.9	59.0	68.2	72.7		
An	59.8	40.0	31.3	26.3		
Or	0.3	1.0	0.5	1.0		

	Biotite	Ilmenite	
	86SF81	86SF75	86SF81
SiO_2	35.36		
TiO_2	4.03	52.13	54.46
Al_2O_3	14.60		
Cr_2O_3	0.01	0.06	0.06
FeO*	25.36	47.38	44.87
MnO	0.16	1.10	2.51
MgO	7.76	0.15	0.10
CaO	0.03		
Na_2O	0.10		
K_2O	8.81		
Total	96.22	100.82	102.00
0 =	11	6	
Si	2.751		
Ti	0.236	1.970	2.012
Al	1.339		
Cr	0.001	0.002	0.002
Fe	1.650	1.991	1.844
Mn	0.010	0.047	0.104
Mg	0.900	0.011	0.007
Ca	0.002		
Na	0.015		
K	0.874		
Mg/Fe	0.55		

sion of petrogenesis. The complete set of analyses will, however, be available upon request from the senior author. Hence, analyses presented in the diagrams of Figs. 9–11 are considered to reflect the liquid evolution. From field evidence it seems reasonable that the basic and felsic dykes are cogentic with the evolution of the gabbronorite/diorite. Thin section studies, however, show that the basic dykes contain appreciable amounts of phenocrysts, particularly plagioclase, and they have therefore been ignored in the further petrogenetic consideration. In the $(Na_2O + K_2O)$ – SiO_2 diagram (Fig. 9A), the data show a subalkaline affinity, and in the AFM diagram (Fig. 9B) they closely follow, with the exception of sample 87–SF–104, the boundary line between the tholeiitic and calc-alkaline series. In Bowen diagrams (Fig. 10), an enrichment of TiO_2, FeO(t) and P_2O_5 occurs as MgO decreases to around 2 wt% (represented by sample 87–SF–104). These elements decrease rapidly at lower MgO values, while SiO_2 increases. CaO shows a marked decrease from ca. 6 wt% MgO, whereas Ni and Cr show a more continuous decrease with decreasing

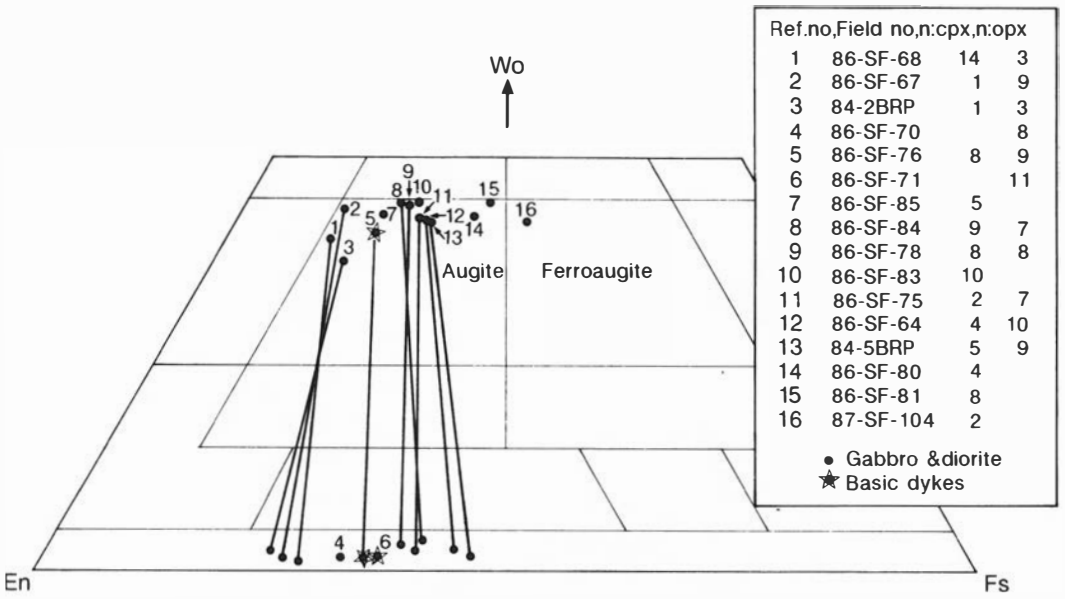

Fig. 5. Composition of pyroxenes expressed in terms of atomic ratio Ca : Mg: Fe. Cpx and opx from the same samples are connected by tie-lines.

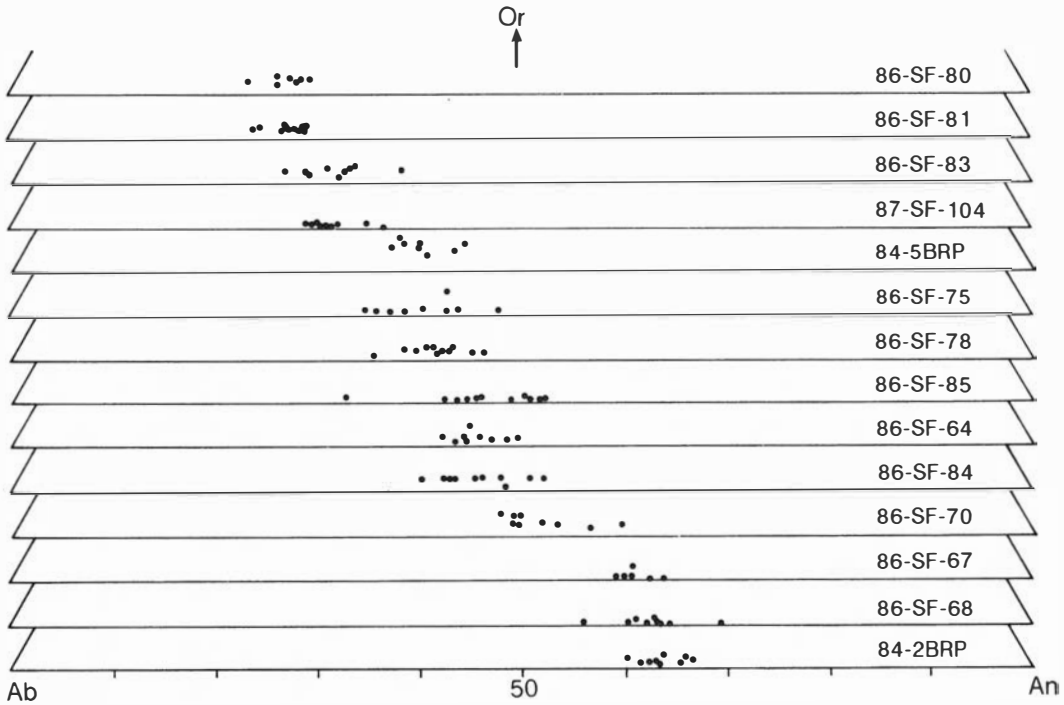

Fig. 6. Composition of plagioclase from gabbronorite and diorites, expressed in terms of Ab–An–Or.

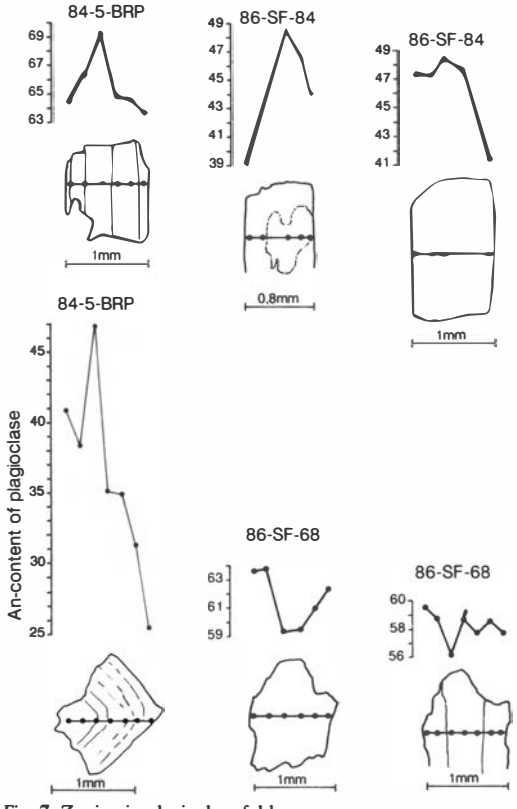

Fig. 7. Zoning in plagioclase feldspars.

MgO. This shows the effects of the removal of olivine and clinopyroxene from the melt. Ba increases progressively as MgO decreases, whereas in the case of Y, Zr, Nb and Ce, these elements reach maximum concentrations at around 2 wt% MgO (Fig. 10).

Discussion

Tectonic environment

Fig. 11. shows the MORB normalized trace-element patterns of the most representative diorites of the GI. From Y through to Rb there is a steady increase in the Rock/MORB ratio, with marked negative anomalies for Ti and Nb. Relative to Rb, there is a marked drop in the concentrations of K and Sr. Such a pattern is typical of subduction-related magmatism (e.g. Thompson et al. 1984; Thorpe et al. 1984; Holm 1985).

Petrogenesis

Clear evidence that fractional crystallization has been operative during the evolution of the GI is provided by the whole-rock geochemistry (Figs. 9, 10), and in particular the compositional ranges

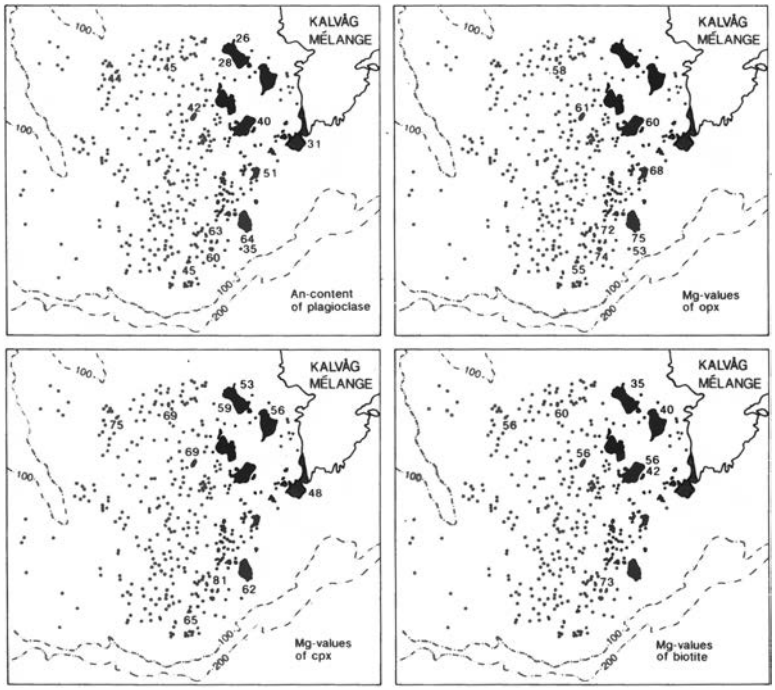

Fig. 8. Map showing the distribution of plagioclase (An content), pyroxene and biotite data (mg values: 100 Mg/(Mg + Fe + Mn)) in the Gåsøy Intrusion (shown in black). The stars show depths between 0 and 10 m, and the 100 and 200 m contour lines are shown. These bathymetric data give some indication about the extent of the unexposed part of the Gåsøy Intrusion.

Table 3. Major and trace element composition of the Gåsøy Intrusion.

Field no.	SiO_2	TiO_2	Al_2O_3	FeO*	MnO	MgO	CaO	Na_2O	K_2O	P_2O_5	LOI	Total
Gabbro and diorite												
86–SF–70	52.50	0.81	16.23	8.86	0.17	9.48	9.28	3.12	0.36	0.08	0.03	100.92
86–SF–75	52.85	1.48	16.39	9.99	0.19	5.99	9.12	3.36	0.56	0.27	0.40	100.60
86–SF–78	52.29	1.84	17.08	9.11	0.17	5.87	8.70	3.36	0.69	0.17	1.10	100.38
86–SF–83	52.71	1.94	16.93	10.40	0.18	5.22	7.79	3.55	1.07	0.43	1.60	101.82
86–SF–81	55.64	1.60	16.60	9.81	0.16	3.27	6.34	3.54	2.33	0.55	0.80	100.64
87–SF–104	52.12	1.83	17.43	11.53	0.17	1.99	6.30	3.13	1.82	0.62	1.50	98.44
Felsic dykes												
86–SF–77	65.18	0.49	17.20	3.98	0.09	1.43	4.15	4.67	2.41	0.21	0.50	100.31
86–SF–79	64.64	0.56	17.10	4.61	0.08	1.24	4.03	4.10	1.96	0.18	0.60	99.10
86–SF–74	68.11	0.42	16.94	2.48	0.04	0.68	3.31	5.06	1.81	0.11	1.00	99.96

Field no.	V	Cr	Ni	Rb	Sr	Y	Zr	Nb	Ba	Ce
Gabbro and diorite										
86–SF–70	126	412	86	0	356	16	41	2	91	0
86–SF–75	195	215	62	1	350	37	92	4	109	10
86–SF–78	234	158	60	10	380	23	98	7	180	8
86–SF–83	257	120	41	18	344	41	122	11	195	35
86–SF–81	163	48	19	87	278	56	326	20	349	97
87–SF–104	183	28	20	41	335	63	501	20	438	107
Felsic dykes										
86–SF–77	64	31	11	65	452	12	137	10	412	47
86–SF–79	70	33	13	57	548	12	193	9	500	60
86–SF–74	45	26	12	59	587	8	189	9	521	70

of plagioclase, pyroxenes and biotite (Figs. 5, 6, 8). In order to test the extent to which fractional crystallization of one or various combinations of minerals controlled the whole-rock geochemical trend, petrographic-mixing calculations based on a modified computer program by Bryan et al. (1969) have been carried out. A large number of possible parent–daughter pairs, combined with appropriate mineral data (Table 2) were tested, and the most plausible alternatives are presented here (Table 5). A further test of the reliability of the proposed models is provided by the calculation of trace-element concentrations, based on the proportion of extracted minerals. For such calculations uncertainties are introduced by the choice of mineral/melt partition coefficients which may show large variations (e.g. Arth & Hanson 1975). Those used for this account are listed in Table 4. To drive the composition of the GI from that of a gabbronorite (sample 86–SF–70) to a typical diorite (sample 86–SF–75), extraction of around 53% of olivine, orthopyroxene, clinopyroxene and plagioclase, of which plagioclase and orthopyroxene dominate, gives a satisfactory result (Table 5a). Also the calculated trace-element concentrations of the parent compare well with the analysed values. Ni shows a somewhat high calculated value, but this is very sensitive to the choice of olivine/melt partition

Fig. 9. $Na_2O + K_2O$ vs. SiO_2 (a) and $Na_2O + K_2O - FeO(t) - MgO$ (b) plots of selected samples from the Gåsøy Intrusion. The boundary line between alkaline and subalkaline fields in (a) is taken from Macdonald & Katsura (1964). The boundary between the tholeiitic (TH) and calc-alkaline (CA) fields of (b) is taken from Irvine & Baragar (1971).

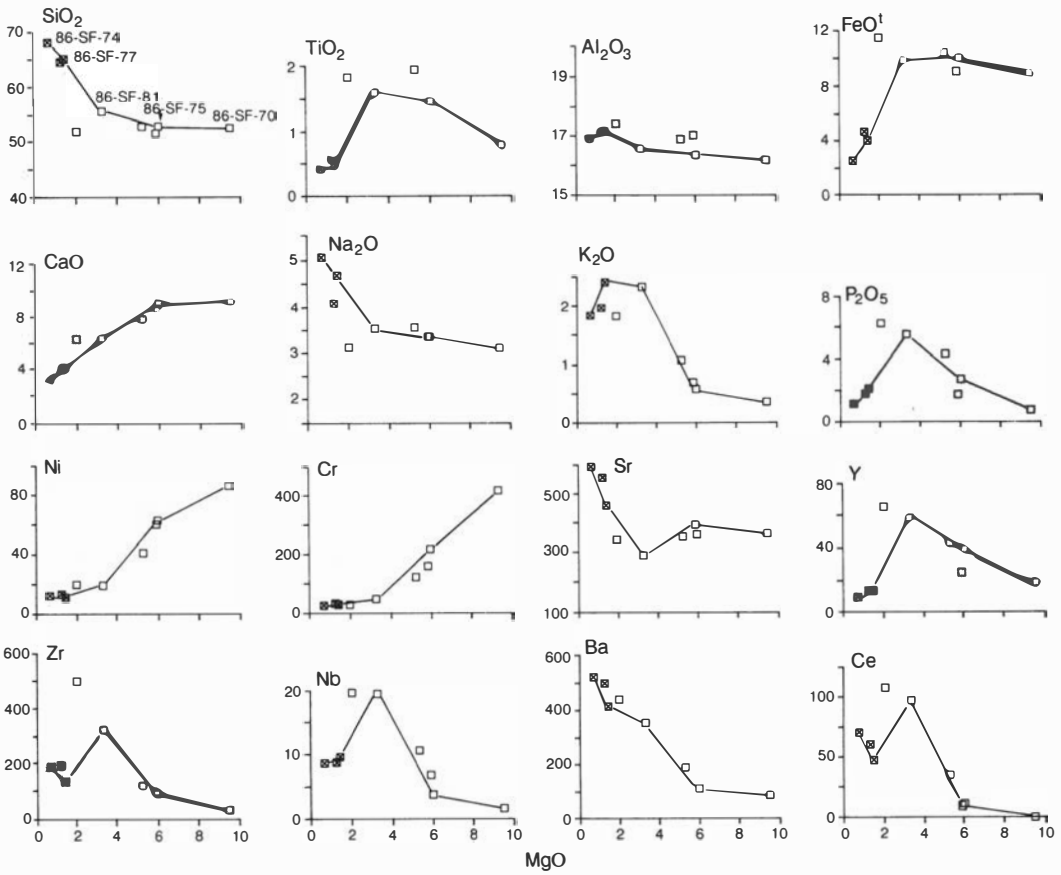

Fig. 10. MgO element diagrams (Bowen diagram) of selected samples from the Gåsøy Intrusion. Samples used as parent–daughter pair in modelling (Table 5a, b) are indicated and connected by tie-lines. Open squares: gabbronorite and diorite. Squares with crosses: Felsic veins.

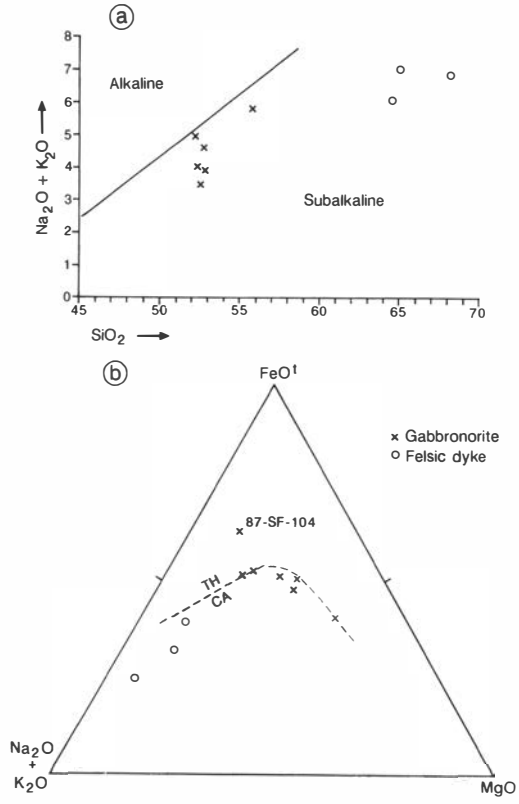

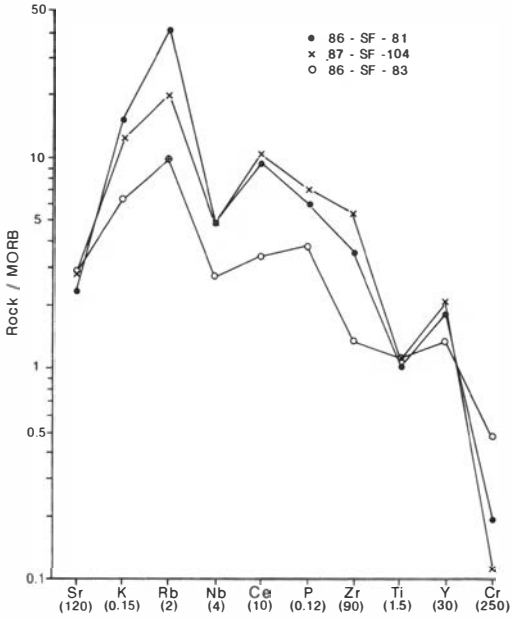

Fig. 11. Trace-element patterns of selected diorite samples from the Gåsøy Intrusion. Average MORB values are taken from Pearce (1980).

Table 4. Mineral/melt partition coefficients used in modelling.

	Ol	Opx	Cpx			Plag		
	(b)	(b)	(b)	(i)	(a)	(b)	(i)	(a)
Ni	10f	4f	2f			0.04c		
Cr	0.2f	2f	10f			0.001f		
Sr	0.016d	0.016d	0.17d			2.2b	2.84a	4.4a
Y	0.01g	0.2g	0.5g	1.5g	4g	0.03g	0.06g	0.1g
Zr	0.01g	0.03g	0.1g	0.23g	0.6g	0.01g	0.03g	0.1g
Nb	0.01g	0.15g	0.1g	0.3g	0.8g	0.01g	0.03g	0.06g
Ba	0.005e	0.011e	0.002e			0.33b	0.36a	0.31a
Ce	0.001d	0.001d	0.04d			0.11b	0.24a	0.27a

	Bi	Amph			Apatite	
	(i)&(a)	(b)	(i)	(a)	(i)	(a)
Ni		3.0f				
Cr		12f				
Sr	0.12a	0.43a		0.02a		
Y	1.23h	1g	2.5g	6g	20g	40g
Zr	1.2h	0.5g	1.4g	4g		
Nb	6.36h	0.8g	1.3g	4g		
Ba	6.36a	0.42a		0.04a		
Ce	3.94h	0.2a		1.52a	34.7a	

Partition coefficients taken from: (a) Arth & Hanson (1975); (b) Drake & Weill (1975); (c) Lindström (1976); (d) Frey et al. (1978); (e) Irvine (1978); (f) Cox et al. (1979); (g) Pearce & Norry (1979); (h) Nash & Crecraft (1985). Partition coefficients for basaltic, intermediate and acid rocks are indicated as (b), (i) and (a), respectively.

Table 5a. Least squares mass balance models for the compositional change from parent (gabbronorite) to derivative (quartz-bearing diorite) by fractional crystallization.

	Deriv.	Obs. Par.	Calc. Par.	Deriv.	Obs. Par.	Calc. Par.	Calc. Par.
	86SF75	86SF70	1	86SF81	86SF75	1	2
SiO_2	52.85	52.50	52.25	55.64	52.85	53.00	52.55
TiO_2	1.48	0.81	0.77	1.60	1.48	2.18	1.67
Al_2O_3	16.39	16.23	16.18	16.60	16.39	15.78	16.17
FeO*	9.99	8.86	8.86	9.81	9.99	9.20	9.71
MnO	0.19	0.17	0.18	0.16	0.16	0.18	0.21
MgO	5.99	9.48	9.40	3.27	5.99	6.29	6.22
CaO	9.12	9.28	9.24	6.34	9.12	8.64	8.92
Na_2O	3.36	3.12	2.84	3.54	3.36	3.71	3.68
K_2O	0.56	0.36	0.28	2.33	0.56	1.00	0.88
P_2O_5	0.27	0.08	0.20	0.55	0.27	0.24	0.24
Percent derivative			47.1			40.8	28.5
Olivine			5.6			7.9	—
Orthopyroxene			12.6			—	—
Clinopyroxene			7.2			16.1	2.8
Plagioclase			27.2			32.9	31.5
Ilmenite			—			2.7	1.3
Amphibole						—	37.4
Sum of squares (r^2)			0.08			2.13	0.42
Observed ( ) and calculated trace element abundances							
Cr	(215)	(412)	414	(48)	(215)	254	57752
Ni	(62)	(86)	165	(19)	(62)	19	42
Sr	(350)	(356)	397	(278)	(350)	370	363
Y	(37)	(16)	19	(56)	(37)	26	32
Zr	(92)	(41)	44	(326)	(92)	137	130
Nb	(4)	(2)	2	(20)	(4)	8	10
Ba	(109)	(91)	59	(349)	(109)	169	157
Ce	(10)	(n.d.)	5	(97)	(10)	42	34

Key to minerals used in mixes: 86–SF–70 (parent) – 86–SF–75 (derivative): Olivine, orthopyroxene and plagioclase from 86–SF–67; clinopyroxene from 86–SF–68. 86–SF–81 (parent) – 86–SF–75 (derivative): Olivine from 86–SF–67; plagioclase and ilmenite from 86–SF–75; clinopyroxene from 86–SF–78; amphibole from 86–SF–85.

coefficient. To generate the more differentiated quartz-bearing diorite (represented by sample 86–SF–81) from the composition of diorite 86–SF–75 is more problematic when taking trace-element concentrations into consideration. In Table 5a two fractionation models are presented, the first one in which plagioclase, clinopyroxene, olivine and minor ilmenite are removed, and the second in which amphibole and plagioclase with minor amounts of clinopyroxene and ilmenite are removed. In terms of major elements, and also with respect to most of the incompatible trace elements, the second model appears to be the most satisfactory. However, in terms of Cr, when applying the partition coefficient for amphibole/melt as given in Table 4, the calculated parent has a concentration which is 269 higher than that of the observed parent. Also, amphibole as euhedral phenocrysts is rare. On this basis, we therefore find it unlikely that amphibole was the main fractionating mineral, and consider the first model as the most plausible.

The generation of granitic liquids by continued crystal fractionation from a quartz-bearing dioritic parent may give reasonable results with respect to major elements, but very poor results with respect to all trace elements (Table 5b). The most fractionated felsic material (sample 86–SF–74, Table 3) may be derived by some 25% crystal fractionation from a liquid with the composition of sample 86–SF–77. Two models are shown in Table 5b in which both plagioclase and biotite are the dominant fractionating minerals. Both models give reasonable results with respect to Sr, Zr, Nb

Table 5b. Least squares mass balance models for the compositional change from parent (quartz-bearing diorite) to derivative (granite) by fractional crystallization.

	Deriv.	Obs. Par.	Calc. Par.	Deriv.	Obs. Par.	Calc. Par.	Calc. Par.
	86SF77	86SF81	1	86SF74	86SF77	1	2
SiO_2	65.18	55.64	55.21	68.11	65.18	65.34	65.29
TiO_2	0.49	1.60	1.63	0.42	0.49	0.62	0.65
Al_2O_3	17.20	16.60	16.26	16.94	17.20	17.19	17.22
FeO*	3.98	9.81	9.68	2.48	3.98	4.15	4.14
MnO	0.09	0.16	0.14	0.04	0.09	0.05	0.05
MgO	1.43	3.27	3.43	0.68	1.43	1.29	1.21
CaO	4.15	6.34	6.24	3.31	4.15	4.08	3.95
Na_2O	4.67	3.54	4.18	5.06	4.67	4.88	4.89
K_2O	2.41	2.33	2.62	1.81	2.41	2.10	2.12
P_2O_5	0.21	0.55	0.61	0.11	0.21	0.32	0.47
Percent derivative			38.3			82.6	84.7
Clinopyroxene			8.6			2.4	—
Plagioclase			27.0			8.6	7.2
Ilmenite			0.9			—	—
Amphibole			8.1			—	1.8
Biotite			18.1			6.7	6.3
Apatite			1.3			0.5	0.9
Sum of squares (r^2)			0.64			0.22	0.34
Observed ( ) and calculated trace element abundances							
Sr	(452)	(278)	590	(587)	(452)	731	625
Y	(12)	(56)	16	(8)	(12)	9	26
Zr	(137)	(326)	91	(189)	(137)	174	179
Nb	(10)	(20)	27	(9)	(10)	12	11
Ba	(500)	(349)	1350	(521)	(500)	693	596
Ce	(60)	(97)	181	(70)	(60)	94	613

Key to minerals used in mixes: 86–SF–81 (parent) – 86–SF–77 (derivative): All mineral data, except apatite, from 86–SF–81. Apatite from Deer et al. (1970) (anal. 1, Table 50). 86–SF–77 (parent) – 86–SF–74 (derivative): Clinopyroxene and plagioclase from 87–SF–104; amphibole and biotite from 86–SF–81; apatite as above.

and Ba, but on the basis of Y of Ce concentrations model 2 seems unrealistic. In all models ilmenite has been excluded from the calculations due to the lack of appropriate partition coefficients.

Magma mixing and crustal contamination may have contributed to the misfits in the mass-balance and trace-element calculations towards the more differentiated members of the GI. A number of samples from the GI have been analysed for Sr isotopes (Table 1), and give evidence that the most differentiated material has suffered crustal contamination. Thus, the isochrons based on acid veins/quartz-bearing diorite, and gabbronorite/diorite/basic dyke, give initial $^{87}Sr/^{86}Sr$ ratios of 0.7052 and 0.7037, respectively. The highest $^{87}Sr/^{86}Sr$ value of the most acid components may thus be a result of contamination by older, more radiogenic material. Field evidence, giving evidence for the production of granitic melts by partial melting of metasediments, support contamination. Various types of zoning in the plagioclase show different magmatic conditions during crystallization. While continuous normal zoning indicates equilibrium fractionation, discontinuous, reverse zoning occurs during superimposed disequilibrium (Loomis 1982). The latter may be caused by magma mixing (e.g. Mørk 1984). This is further suggested by the mantling of feldspar (Hibbard 1981).

Concentric zoning with increasing acidity towards the core is most commonly observed in mesozonal plutons (e.g. Tindle & Pearce 1981; Stephens et al. 1985). From the limited data, confined largely to a small part of the margin of

the GI, which on the basis of bathymetry (Fig. 8) may be of considerably larger size than that shown in Fig. 1, it may be suggested that the GI represents a zoned intrusion in which the bottom part consists of layered gabbronorite and the upper part of diorites. The GI may thus largely represent the products of fractional crystallization modified by some unquantified amount of crustal contamination and magma mixing.

Conclusions

The main features of the Gåsøy Intrusion may be summarized as follows:

1. Its central to lower part consists of massive to banded/layered gabbronorite interlayered with wehrlite and diorite. The upper part consists of massive, medium to coarse grained diorite, grading progressively into more differentiated quartz-bearing diorite and finally granite towards the contact with its host (the Kalvåg Melange).
2. A Sm–Nd mineral isochron (based on separated plagioclase, clinopyroxene and apatite) from the diorite yields an age of 380 ± 26 Ma. Rb–Sr whole-rock dating of several samples gives similar ages.
3. The trends defined by the major elements and mineralogical compositions indicate a transitional character between calc-alkaline and tholeiitic affinities. The trace-element patterns, in particular the negative Ti and Nb anomalies, show clear evidence of subduction.
4. Least-squares, mass-balance modelling combined with comparison between observed and calculated trace-element abundances indicate the following: (a) To change the compositions from a gabbronorite (MgO ca. 9.5 wt%) to a diorite (MgO ca. 6 wt%) would indicate ca. 53% fractional crystallization of olivine (10%), plagioclase (52%), orthopyroxene (24%) and clinopyroxene (14%).

   (b) To change the diorite composition from a MgO content of 6 wt% to ca. 3.3 wt% requires a further 59% fractional crystallization of olivine (13.5%), ilmenite (4.5%), plagioclase (55%) and clinopyroxene (27%).

   (c) To further change the liquid from a diorite (MgO ca. 3.3 wt%) to a granitic composition (MgO ca. 1.4 wt%) may be achieved by a further about 60% fractional crystallization of plagioclase (42%), ilmenite (1.5%), clinopyroxene (13.5%), amphibole (12.5%), biotite (28.5%) and apatite (2%). However, calculated trace-element concentrations show large deviations from observed values. Evidence of crustal contamination (Sr isotopes) and magma mixing (zoning and mantling of feldspars) might have contributed to the poor results.

Acknowledgements. – Financial support for this study has been provided through grants (D.41.31.147) from the Norwegian Research Council for Science and the Humanities. We thank B. Robins, T. B. Andersen and the reviewers (E. R. Neumann and one anonymous reviewer) for constructive discussions and comments. Else Lier kindly prepared the illustrations. This work is publication no. 76 in the International Lithosphere Project (ILP).

Manuscript received April 1989

References

Arth, J. G. & Hanson, G. N. 1975: Geochemistry and origin of the early Precambrian crust of northern Minnesota. *Geochimica et Cosmochimica Acta 39*, 325–362.

Bryan, W. B., Finger, L. W. & Chayes, F. 1969: Estimating proportions in petrographic mixing equations by least-squares approximation. *Science 163*, 926–927.

Bryhni, I. & Lyse, K. 1985: The Kalvåg Melange, Norwegian Caledonides. *In* Gee, D. G. & Sturt, B. A. (eds.): *The Caledonian Orogen – Scandinavia and Related Areas*. J. Wiley, New York, 417–427.

Colby, J. B. 1968: MAGIC IV – a computer program for quantitative electron microprobe analysis. *X-Ray Analyses 11*, 287–306.

Cox, K. G., Bell, J. D. & Pankhurst, R. J. 1979: *The Interpretation of Igneous Rocks*. George Allen & Unwin. London. 450 pp.

Deer, W. A., Howie, R. A. & Zussman, J. 1970: *An Introduction to the Rock Forming Minerals*. Longman, London. 528 pp.

Drake, M. J. & Weill, D. F. 1975: Partition of Sr, Ba, Ca, Eu^{2+}, Eu^{3+} and other REE between plagioclase feldspar and magmatic liquid: an experimental study. *Geochimica et Cosmochimica Acta 39*, 689–712.

Dunning, G. R. & Pedersen, R. B. 1988: U/Pbages of ophiolites and arc-related plutons of the Norwegian Caledonides: Implications for the development of Iapetus. *Contributions to Mineralogy and Petrology 98*, 13–23.

Flanagan, F. J. 1973: 1972-values for international geochemical reference standards. *Geochimica et Cosmochimica Acta 37*, 1189–1200.

Frey, F. A., Green, D. H. & Roy, S. D. 1978: Integrated models of basalt petrogenesis: A study of quart tholeiites to olivine melilitites from South Eastern Australia utilizing geochemical and experimental petrological data. *Journal of Petrology 19*, 463–513.

Hibbard, M. J. 1981: The magma mixing origin of mantled feldspar. *Contributions to Mineralogy and Petrology 76*, 158–170.

Holm, P. E. 1985: The geochemical fingerprints of different tectonomagmatic environments using hygromagmatophile

element abundances of tholeiitic basalts and basaltic andesites. *Chemical Geology 51*, 303–323.

Irvine, T. N. & Baragar, W. R. A. 1971: A guide to the classification of the common volcanic rocks. *Canadian Journal of Earth Science 8*, 523–548.

Irvine, A. J. 1978: A review of experimental studies of crystal/liquid trace element partitioning. *Geochimica et Cosmochimica Acta 42*, 743–770.

Kolderup, N-H. 1928: Fjeldbygningen i kyststrøket mellom Nordfjord og Sognefjord. *Årbok Bergens Museum, Matematisk Naturvitenskapelige rekke 1*, 1–221.

Leake, B. E. 1978: Nomenclature of amphibolites. *Mineralogical Magazine 42*, 533–563.

Lindström, D. J. 1976: Experimental study of the partitioning of the transition metals between clinopyroxene and coexisting silicate liquids. PhD thesis, University of Oregon.

Loomis, T. P. 1982: Numerical simulations of crystallization processes of plagioclase in complex melts: the origin of major and oscillatory zoning in plagioclase. *Contributions to Mineralogy and Petrology 81*, 219–229.

Macdonald, G. A. & Katsura, T. 1964: Chemical composition of Hawaiian lavas. *Journal of Petrology 5*, 82–133.

Mearns, E. W. 1986: Sm–Nd ages for Norwegian garnet peridotites. *Lithos 19*, 269–278.

Mørk, M. B. E. 1984: Magma mixing in the post-glacial Veidivøtn fissure eruption, southeast Iceland: a microprobe study of mineral and glass variations. *Lithos 17*, 55–75.

Nash, W. P. & Crecraft, H. R. 1985: Partition coefficients for trace elements in silicate magmas. *Geochimica et Cosmochimica Acta 49*, 2309–2322.

Padfield, T. & Gray, A. 1971: Major element rock analyses by X-ray fluorescence – a simple fusion method. N.V. Philips, Analytical Equipment FS35, Eindhoven.

Pearce, J. A. 1980: Geochemical evidence for the genesis and eruptive setting of lavas from Tethyan ophiolites. *Proceedings of the International Ophiolite Symposium, Nicosia 1979*, 261–272.

Pearce, J. A. & Norry, M. J. 1979: Petrogenetic implications of Ti, Zr, Y and Nb variations in volcanic rocks. *Contributions to Mineralogy and Petrology 69*, 33–47.

Reed, S. J. B. 1975: *Electron Microprobe Analyses*. Cambridge University Press, London, 400 pp.

Reusch, H. 1903. Forsteininger i fjeldet på Frøyen. *Naturen 7*, 160.

Stephens, W. E., Whitney, J. E., Thirlwall, M. F. & Halliday, A. N. 1985: The Crifell zoned pluton: correlated behaviour of rare element abundances with isotopic system. *Contributions to Mineralogy and Petrology 89*, 226–238.

Thompson, R. N., Morrison, M. A., Hendry, G. L. & Parry, S. J. 1984: An assessment of the relative roles of crust and mantle in magma genesis: an elemental approach. *Philosophical Transactions of the Royal Society of London A 310*, 549–590.

Thorpe, R. S., Francis, P. W. & O'Callaghan, L. 1984: Relative roles of source composition, fractional crystallization and crustal contamination in the petrogenesis of Andean volcanic rocks. *Philosophical Transactions of the Royal Society of London A 310*, 675–692.

Tindle, A. G. & Pearce, J. A. 1981: Petrogenetic modelling of in situ fractional crystallization in the zoned Loch Doon Pluton, Scotland. *Contributions to Mineralogy and Petrology 78*, 196–207.